Liquid–Solid Mass Transfer in a Three-Phase Stationary Catalytic Basket Reactor

Marijana Mitrovic, Isabelle Pitault, and Michel Forissier
Laboratoire de Génie des Procédés Catalytiques, CNRS-CPE, BP 2077, 69616 Villeurbanne Cedex, France

Serge Simoens
Laboratoire de Mécanique des Fluides et d'Acoustique, CNRS-ECL, 69134 Ecully Cedex, France

Didier Ronze
Dépt. de Génie Chimique–Génie des Procédés, Université Claude Bernard, Lyon I, IUT A, 69622 Villeurbanne Cedex, France

DOI 10.1002/aic.10436
Published online April 22, 2005 in Wiley InterScience (www.interscience.wiley.com).

Measurements of the liquid–solid mass transfer coefficient k_S were performed in a three-phase multiple impeller and stationary catalytic basket reactor, called a Robinson–Mahoney reactor. Local coefficients were determined using naphtol particle dissolution in water and n-heptane with or without gas flow. Experiments have shown that local coefficients $k_{S\,loc}$ depend on the particle position in the basket, agitation speed, and liquid properties. A correlation linking k_S to liquid velocity was established in a reactor simulating hydrodynamics in a piece of catalytic basket. Liquid velocity values were validated using a particle image velocimetry technique in a Robinson–Mahoney reactor, using water. © 2005 American Institute of Chemical Engineers *AIChE J,* 51: 1747–1757, 2005
Keywords: Robinson–Mahoney reactor, mass transfer, liquid–solid transfer, catalytic basket, particle image velocimetry (PIV)

Introduction

Determination of three-phase reaction intrinsic kinetics (such as gas oil hydrocracking) is a crucial step to enhance development and understanding of the process. Choosing the best laboratory reactor for kinetic studies remains a complex task, insofar as measured data should be controlled only by chemical kinetics and not blurred by purely physical processes such as mass transfer. Many three-phase reactors, including catalysts with several shapes and sizes, have been reviewed (Dudukovic et al., 2002; Turek et al., 1983; Weekman, 1974). Weekman (1974) showed that fixed-bed reactors present some drawbacks, such as difficulty in achieving uniform temperatures in a granular bed, and that stirred basket reactors should present more advantages. The catalytic basket reactors can be classed in two groups: (1) spinning or stirred basket reactor, first designed by Carberry (1964); and (2) stationary basket reactor, designed by Robinson and Mahoney (Mahoney, 1981) and then modified and provided by Autoclave Engineers Company and so-called Robinson–Mahoney (RM) catalyst testing reactor. Although, for some spinning or stirred basket reactors, characterization of transport phenomena has been studied and published (Kawakami et al., 1976; Kenney and Sedricks, 1972; Mahoney et al., 1978; Ohta et al., 1980), Vanrysselberghe and Froment (1996) reported that they verified the complete mixing in the Robinson–Mahoney's reactor only by residence time distribution studies.

The RM reactor, specifically intended to offer an optimal contact between gas and liquid and liquid and solid, consists of a multiple impeller located inside a stationary catalytic basket, which provides the fluid flow through the basket (that is, in the catalyst bed). This reactor seems to present some advantages in

Correspondence concerning this article should be addressed to I. Pitault at Isabelle.Pitault@lgpc.cpe.fr.

kinetic studies (Schweitzer et al., 1999; Trasobares et al., 1998; Vanrysselberghe and Froment, 1996): among the advantages could be cited direct rate measurements in steady-state conditions and use of the same catalyst particles as in industrial units. Nevertheless, the high liquid–solid transfer in a stirred tank reactor (compared with that in a trickle-bed reactor) mainly arises from the small size of catalyst particles (Pangarkar et al., 2002). Therefore, the use of large extruded articles could drastically reduce liquid–solid transfer in the RM reactor. This phenomenon should be increased by the pressure drop induced by the basket wall that should decrease the fluid velocities. Regarding the gas–liquid mass transfer, the effects induced by the basket (which includes baffles) on gas hold-up and bubble sizes compared with those in a stirred tank reactor are not so obvious. In spite of those reflections, which could be considered as very simplistic, the limits of chemical control have not been thoroughly explored and still remain unclear or even unknown in the RM reactor. Trickled-bed reactors do not provide the best conditions under which to compare extruded catalysts without external limitations for some fast chemical reactions [as well as for hydrodesulfurization (HDS) reactions on new generation of catalyst at the reactor top]; thus it is of paramount interest to know whether the use of RM reactors is more appropriate for those reactions or if a stirred tank reactor is the only suitable reactor.

This article focuses on solid–liquid mass transfer in a Robinson–Mahoney reactor (a future report will explore the gas–liquid transfer). The first step of this study was a parametric investigation in the Robinson–Mahoney reactor to estimate global and local mass-transfer coefficients as a function of solvent properties and location in the basket. Then a "catalytic basket simulation device" (CBSD) was used to correlate the mass-transfer coefficient with the liquid velocity through a section of the catalytic basket. The last step consisted in measuring fluid flow velocities inside the RM reactor, using the particle image velocimetry (PIV) technique previously used in liquid-phase agitated vessels to determine local velocity profiles (Lafontaine and Shepherd, 1996; Lamberto et al., 1999), that rely on and corroborate the two previous sets of results. These measurements, coupled to CBSD results, were expected to corroborate the mass-transfer correlation in the Mahoney–Robinson reactor. Finally, solid–liquid mass-transfer rates should be compared to the chemical rates found in gas oil hydrocracking studies.

Evaluation of the solid–liquid mass transfer coefficient (k_S) has often been performed—because of its simplicity—by solid dissolution (Dutta and Pangarkar, 1993; Evans and Gerald, 1953). The procedure consists in introducing solid particles into the liquid and monitoring the dissolved solid concentration. Water was often used as the liquid phase. A wide range of solids was used, such as β-naphtol, potassium permanganate, benzoic acid (Sano et al., 1974), and potassium sulfate (Grisafi et al., 1998). Organic solvents were scarcely studied (Levins and Glastonbury, 1972). Patil et al. (1984) and Levins and Glastonbury (1972) studied the effects of gas bubbles on solid–liquid mass transfer by using metal dissolution in acidic aqueous solutions. The solubility of the solid must remain low to avoid the interfacial area variation; this requirement led us to choose β-naphtol, the solubility of which is low in both studied solvents (water and *n*-heptane). *n*-Heptane is of a particular interest because its physical properties at room temperature

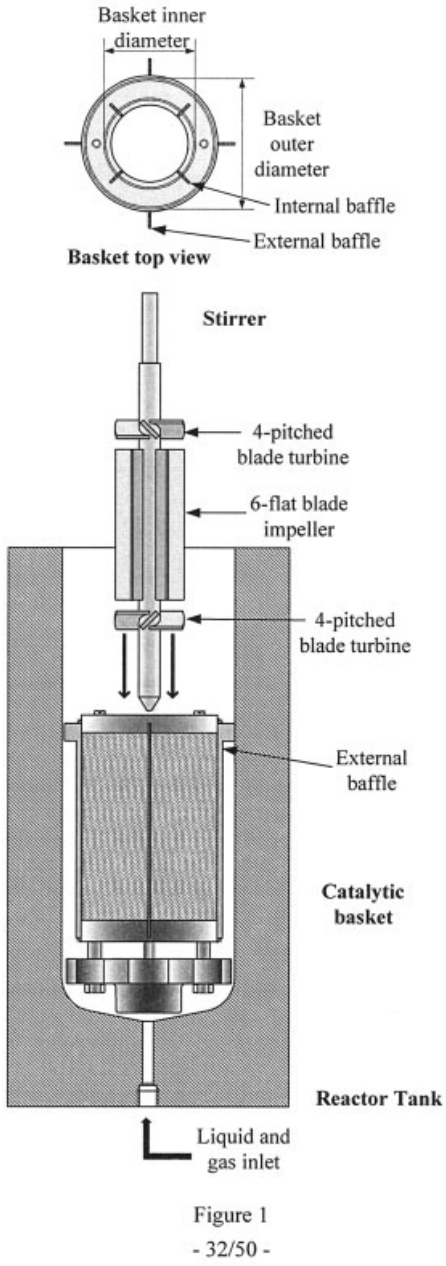

Figure 1
- 32/50 -

Figure 1. Robinson–Mahoney (RM) reactor tank with stationary catalytic basket and stirrer.

(viscosity, specific gravity) are close to those of synthetic gas oil in reaction conditions (380°C, 15 MPa) (Schweitzer, 1998). It should be underlined that those methods have been applied in classical packed-bed or slurry reactors, but not yet in the Robinson–Mahoney reactor.

Experimental Setups

In this work, three setups were used: (1) a cold-flow reactor model that simulates the Robinson–Mahoney reactor (to estimate local and global transfer coefficients in the basket, solvent properties, rotation speed, etc.); (2) the CBSD (the setup composed of a packed-bed reactor including a layer of some catalyst particles to link velocity and transfer coefficients); and (3)

Table 1. Dimensions of Reactor Tank, Basket, Impeller, and Blades

Inner diameter of of reactor tank	0.080 m
Inner height of reactor tank	0.220 m
Height of fixed annular catalytic basket	0.104 m
Inner diameter of fixed annular catalytic basket	0.043 m
Outer diameter of fixed annular catalytic basket	0.059 m
Length of flat blades	0.07 m
Width of flat blades	0.011 m
Angle between two flat blades	60°
Height of the pitched-blade turbine	0.007 m
Diameter of the pitched-blade turbine	0.03 m
Interval between pitched-blade turbine and flat-blade turbine	0.005 m
Diameter wire of the basket screen	5.5×10^{-4} m
Mean opening of the basket screen	9.8×10^{-4} m (16 mesh)
Height of internal and external baffles	0.104 m
Width of internal and external baffles	0.008 m
Angle between two baffles	45°

a PIV-adapted cold-flow reactor model (to measure the local velocities outside of the basket by PIV).

The cold-flow reactor model, adapted from the Robinson–Mahoney reactor (Mahoney, 1981) provided by Autoclave Engineers, consisted of a transparent tank made from polymethylmethacrylate (PMMA), containing a fixed annular catalytic basket and an adapted turbine. The turbine caused liquid to flow through the basket to the reactor wall and induced an upward and a downward stream outside the basket. The multi-impeller consisted of two inverse turbines with four pitched blades surrounding one turbine with six flat blades. To prevent vortexing, the catalytic basket was fitted out with eight baffles: four baffles inside and four baffles outside the basket. The scheme and dimensions of reactor tank, basket, impeller, and blades are given Figure 1 and Table 1, respectively. The liquid volume (V_L) in the reactor tank was 0.89 ± 0.01 L. The gas inlet and outlet were located, respectively, at the bottom and at the top of the vessel. Although the RM reactor was used classically as a continuous reactor during kinetics experiments, we used it as a batch reactor for the liquid phase and as a continuous reactor for the gas phase, to estimate transfer coefficients. For PIV experiments, the reactor was used as a batch reactor (closed on gas and liquid flows).

To measure local mass-transfer coefficient ($k_{S\,loc}$) in the cold-flow RM reactor model, the basket was filled with a layer of cylindrical naphtol particles surrounded by PMMA cylinders with dimensions identical to those of naphtol particles to simulate the catalyst. Each layer contained about 200 naphtol particles and was about 0.01 m thick. The total external area of the naphtol particles introduced in the basket (A_S) was about 0.076 m^2. The void fraction in the basket was about 0.47 (±0.05). To prepare naphtol particles, naphtol was melted then hardened in cylindrical PTFE casts. Naphtol and PMMA particle characteristics are given in Table 2. Local mass-transfer coefficients were measured at several heights in the basket (given in Table 3).

Table 2. Characteristics of Particles

Characteristic	PMMA Particle	Naphtol Particle
Diameter (m)	2.17×10^{-3}	2.0×10^{-3}
Length (m)	6.1×10^{-3}	5.8×10^{-3}
Diameter of the sphere of same area (m)	3.9×10^{-3}	3.7×10^{-3}
Specific gravity (kg m^{-3})	1200	1300

Table 3. Heights of Naphtol Particles in the Catalytic Basket for Local Mass Transfer Coefficients in the Two Liquid Phases: Water and *n*-Heptane

In Water	In *n*-Heptane
0.003 m	0.003 m
0.016 m	
0.046 m	0.041 m
0.076 m	
0.084 m	0.085 m

To measure the global mass-transfer coefficient ($k_{S\,glob}$) in the cold-flow RM reactor model, the basket was completely filled with cylindrical naphtol particles. In this case, the total external area of the naphtol particles (A_S) introduced in the basket was about 0.12 m^2 and the void fraction in the basket was about 0.49 (±0.05).

In both cases, the "catalyst" bed was 0.09 m high and volume of the basket filled with particles was 98×10^{-6} m^3. Some naphtol particles could be crumbled during filling of the basket, and so to avoid the resulting bias in the liquid–solid area, the basket was first watered to dissolve the fines and then dried. The experimental procedure was as follows: the basket, filled with naphtol particles and with/without PMMA particles, was introduced in the tank. The liquid phase (water or *n*-heptane) was then introduced in the tank, the reactor was closed, and the turbine was started. This last event defined the initial time. During experiments, liquid samples were analyzed. The first experiments were achieved without any gas flow. The agitation speed was fixed between 500 and 1500 rpm. The effect of gas flow on $k_{S\,glob}$ in water was studied at 1000 rpm using a nitrogen flow of 5 mL s^{-1}.

The CBSD, designed to reproduce the liquid flow through the basket (Figure 2), was thus made of a thin layer of 40 naphtol particles (previously described) inserted between two screens, similar to the RM basket apparatus, located perpendicularly to liquid flow (Figure 3). The naphtol bed was 0.045 m thick; the void fraction was about 0.47 (±0.05); and 8 cm of inert glass beads above and below the naphtol bed were used to achieve plug flow. A peristaltic pump at the column inlet provided controlled flow of pure liquid. At the column outlet, liquid (water or *n*-heptane) was

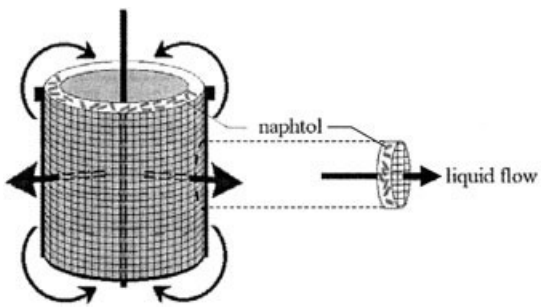

Figure 2. Relation between RM reactor and naphtol bed in CBSD.

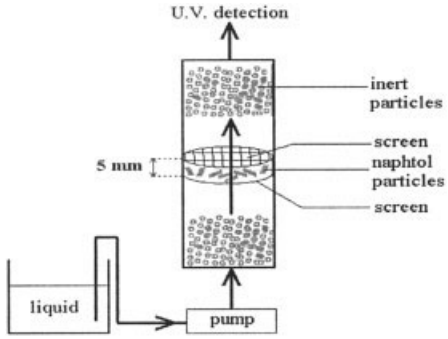

Figure 3. Catalytic basket simulation device (CBSD) setup.

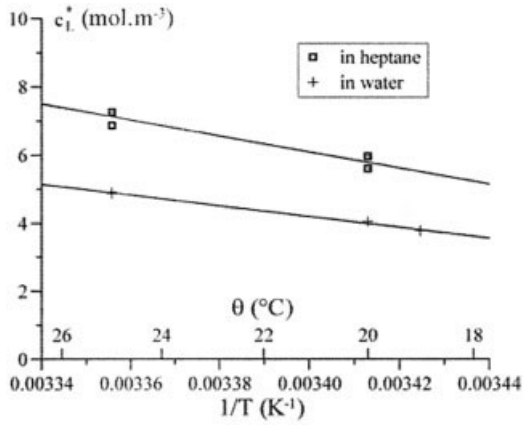

Figure 4. Dissolved naphtol concentration in equilibrium vs. 1/*T*.

sampled and analyzed (using the above-described method). Experiments were performed using liquid interstitial velocities between 10^{-3} and 20×10^{-3} m s^{-1}.

To measure mass-transfer coefficients in the cold-flow RM reactor model or in the CBSD, distilled water and *n*-heptane were used. Liquid properties are reported in Table 4.

Analyses of dissolved naphtol in liquid samples (water or *n*-heptane) were carried out using a UV spectrometer (Perkin Elmer UV/Vis spectrometer, Lambda 2S). Maximal naphtol absorbance in water or *n*-heptane is at 273 nm. Before their analysis, liquid samples were diluted (dilution factor of 20) to use the linear part of the calibration curve. The estimated error made on the naphtol concentration measurement is about 2%. Equilibrium solubility c_L^* was determined using an excess of solid naphtol in contact with the liquid phase (water or *n*-heptane) maintained at a constant temperature between 292 and 298 K. Figure 4 illustrates the results.

A laser PIV technique, used to determine the instantaneous 2-D velocity field for different successive instants, different vertical planes, and different rotation speeds, is well known (Simoens and Ayrault, 1994; Willert and Gharib, 1991) and has been used for increasingly complex experimental configurations (Vincont et al., 2000) such as a stirred vessel (Lafontaine and Shepherd, 1996; Lamberto et al., 1999). The cold-flow RM reactor model environment was adapted to generate a sheet of light whose thickness was about 200 μm. A TSI® PIV system (with a CCD camera of 1016×1000 pixels) was used to acquire and analyze digitized images. The time interval between two successive instants varied from 0.4 to 1.6 ms, depending on the rotation speed. A spatial resolution of 70 μm per pixel was used. The CCD camera was focused successively on three vertical locations to describe a complete vertical plane. The Whittaker subpixel analysis (Lourenco and Krothapalli, 1995) was used to improve the results at 1/10 pixel accuracy. Because of low velocities [few centimeters per second for our rotation speed range (500, 1000, and 1500 rpm)], some specific solid spherical particles of 7.9 μm mean diameter and 1.2×10^{-3} kg m^{-3} were synthesized with polymethylmethacrylate (PMMA) to avoid bias error stemming from gravity. An acquisition frequency of 10 Hz and 200 samples were used to obtain mean velocity and turbulent kinetic energy data. To measure the three velocity vector components (radial u_R, tangential u_T, and vertical u_V) two perpendicular vertical irradiation planes were used (Figure 5): one normal to the basket and the second tangential to the basket wall. At the intersection of the planes it was possible to determine the three velocity components. The analysis was limited to locations between the catalytic basket and the wall. No information was determined inside the catalytic basket or close to the stirrer.

Table 4. Liquid Properties at 298 K

Liquid	Water	*n*-Heptane
Viscosity of liquid phase (10^{-3} Pa · s)	0.91	0.39
Specific gravity of liquid phase (kg m^{-3})	1000	677
Diffusivity of naphtol in liquid (m^2 s^{-1})*	0.76×10^{-9}	2.8×10^{-9}

*From Wilke and Chang (1955), modified by Hayduk and Laudie (1974).

Results and Discussion

Solid–liquid mass transfer in cold-flow RM reactor model

As stated previously, the mass-transfer coefficient was determined from dissolution experiments of naphtol in water and in *n*-heptane. According to Schweitzer et al. (1999) and to our own experimental confirmation (Forissier et al., 2001), the liquid phase was perfectly mixed. Therefore naphtol mass balance can be written as (with the interface supposed to be at thermodynamical equilibrium)

$$V_L \frac{dc_L}{dt} = k_S A_S (c_L^* - c_L) \tag{1}$$

where c_L and c_L^* are the dissolved naphtol concentrations in the bulk and at the liquid side of the liquid–solid interface, respectively; V_L is the volume of the liquid phase; A_S is the total external area of the solid particles; and k_S is the global or local liquid–solid mass transfer coefficient. Because the naphtol solubility is very low (either in water or in *n*-heptane; cf. Figure 4), the external particle area remained almost constant. Equation 1 can be then integrated as

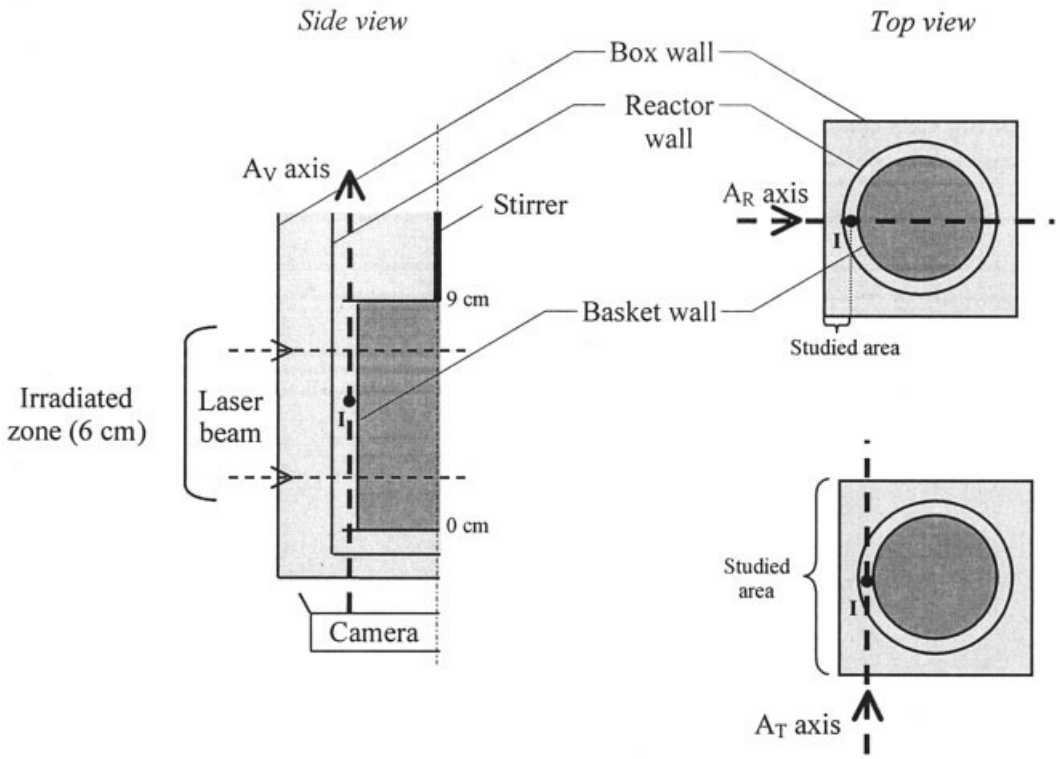

Figure 5. Projection axes used to measure the three vector components of velocity.

$$c_L = c_L^* - (c_L^* - c_{Lo})\exp\left[-\frac{k_S A_S (t - t_o)}{V_L}\right] \qquad (2)$$

where c_{Lo} is the dissolved naphtol concentration at time t_o. The minimization of the residual sum of squares between calculated and experimental values of $c_L(t)$ leads to the expected k_S value. For instance, Figure 6 shows the fitting between the model and experimental data.

Global mass-transfer coefficients were studied for different experimental parameters: agitation speed (N) and gas flow (Q_G) (Figure 7). As shown in Figure 7a, the global mass-transfer coefficient in water without gas is a quasi-linear function of the agitation speed. Regarding the effect of gas flow rate (Figure 7b), experimental uncertainties permit only to conclude that the mass-transfer coefficient increases slightly when a gas phase is present in the liquid phase. This effect could be attributed to a similar phenomenon observed in packed beds: the increase of gas flow rate (as dispersed phase) induces an increase of interstitial liquid velocity and consequently liquid–solid mass transfer (Nosier et al., 1997; Sedahmed et al., 1996; Zarraa et al., 1994).

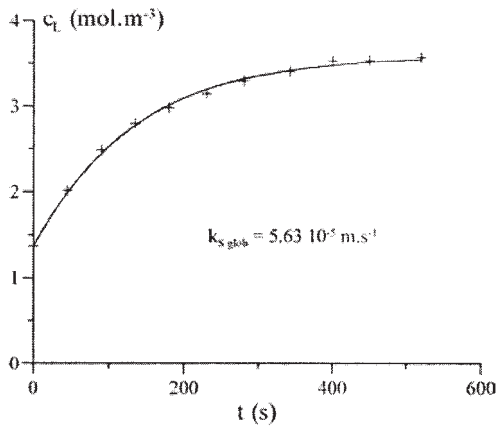

Figure 6. Comparison between model and experimental values (1000 rpm; water).

These global values may hide a heterogeneous profile of the mass transfer along the height of the catalytic basket. Three zones were mainly considered for local mass transfer measurements ($k_{S\,loc}$): at top, center, and bottom of the basket.

The liquid-phase concentration range remained much lower in this case compared to the former one, because of the lower transfer area; the experiments were therefore longer and the temperature variations in the solution (as a result of stirring) could no longer be ignored. Their effects on equilibrium concentration c_L^* were evaluated using a linear relationship (Figure 8), for each experimental condition. Using this relation ($c_L^* = \alpha t + \beta$), Eq. 1 can then be integrated as

$$c_L = \alpha t + \beta - \left(\beta - \frac{\alpha V_L}{k_{S\,loc} A_S}\right)\exp\left(-\frac{V_L}{k_{S\,loc} A_S}\, t\right) - \frac{\alpha V_L}{k_{S\,loc} A_S} \qquad (3)$$

The minimization of the residual sum of squares between calculated and experimental values of $c_L(t)$ leads to the expected $k_{S\,loc}$ value.

Measured mass-transfer profiles are summarized in Figure 9. These profiles reflect the central turbine consisting of six flat blades, which promotes radial flow through the basket at its

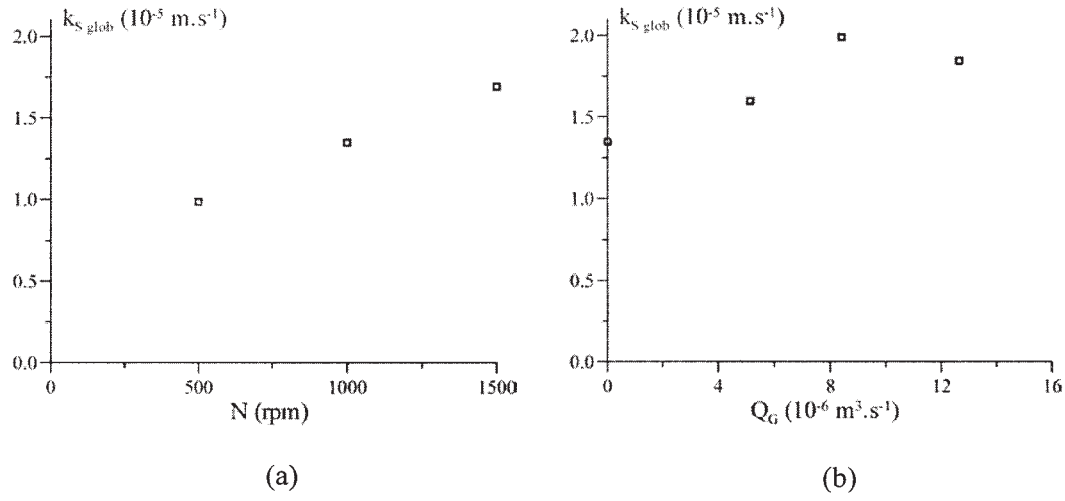

Figure 7. Influence of operating parameters (naphtol/water) on global mass-transfer coefficient.

(a) Mixing speed (Q_G = 0 m^3 s^{-1}); (b) gas flow rate (N = 1000 rpm).

center. Mean values calculated from the profiles measured in water ($k_{S\,loc}^{\text{mean}}$) can be compared to the global coefficients (see Table 5, which also gives the mean local $k_{S\,loc}^{\text{mean}}$ values in the case of *n*-heptane). Given that the uncertainty of these values can be estimated at about 25 to 30%, the difference between the two sets of coefficients is not as great as it seems and can be attributed to a difference in packing, and thus in void degree, between the two sets of experiments.

The whole set of $k_{S\,loc}^{\text{mean}}$ values (in water and in *n*-heptane) can be represented through the following general correlation

$$\text{Sh} = C\,\text{Re}_t^m \text{Sc}^n \tag{4}$$

where $\text{Sh} = (k_S d_{pa})/D_L$ is the Sherwood number, calculated with the diameter of the sphere of same external area than the naphtol particle (d_{pa}); $\text{Re}_t = (N\rho_L d_t^2)/\mu_L$ is the Reynolds number of the turbine with diameter d_t, at agitation speed N; $\text{Sc} = \mu_L/(\rho_L D_L)$ is the Schmidt number; ρ_L and μ_L are the specific gravity and the dynamic viscosity of the fluid, respectively; and D_L is the naphtol diffusivity in the liquid phase.

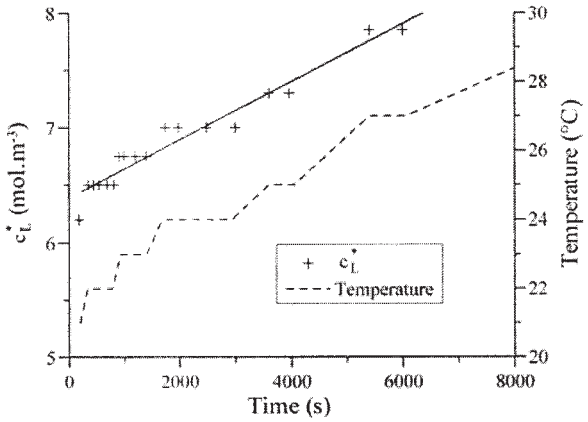

Figure 8. Influence of temperature on equilibrium concentration.

n-Heptane, 1000 rpm, height 4 cm.

Within our experimental range ($8200 \le \text{Re}_t \le 40{,}000$; $200 \le \text{Sc} \le 1200$), correlation 4 becomes

$$\text{Sh} = 4.42 \times 10^{-3} \text{Re}_t^{0.80} \text{Sc}^{1/3} \tag{5}$$

The correlation relevance is shown on the parity diagram (Figure 10).

The observed differences in mass-transfer coefficients, between water and heptane (Figure 9) are of some importance and the mass-transfer coefficient ratios $k_{S\,loc}^{\text{heptane}}/k_{S\,loc}^{\text{water}}$ are almost constant along the basket ($k_{S\,loc}^{\text{heptane}}/k_{S\,loc}^{\text{water}} \approx 4$; cf. Figure 11), and are mainly related to the differences of physical properties of the liquids. Actually, Eq. 5 leads to the following ratio

$$\frac{\text{Sh}_{\text{heptane}}}{\text{Sh}_{\text{water}}} = \left(\frac{\text{Re}_{t\,\text{heptane}}}{\text{Re}_{t\,\text{water}}}\right)^{0.80} \left(\frac{\text{Sc}_{\text{heptane}}}{\text{Sc}_{\text{water}}}\right)^{1/3}$$

From the physical characteristics given in Table 4, it becomes

$$\frac{k_S^{\text{heptane}}}{k_S^{\text{water}}} = \left(\frac{D_{\text{heptane}}^{\text{naphtol}}}{D_{\text{water}}^{\text{naphtol}}}\right)^{2/3} \left(\frac{\rho_{\text{heptane}}}{\rho_{\text{water}}}\right)^{0.47} \left(\frac{\mu_{\text{heptane}}}{\mu_{\text{water}}}\right)^{-0.47} = 3.0$$

which represents an important part of the ratios shown in Figure 11.

The particular behavior of this ratio at 1000 rpm and 4 cm height could be qualitatively linked to a "critical velocity," above which mass transfer increases drastically; that "critical velocity"—depending probably on physical properties of the fluid [and being supposedly between 1000 and 1500 rpm for water (respectively 500 and 1000 rpm for *n*-heptane)]—may be reached in *n*-heptane only at the center of the basket (where the velocity is the highest).

Correlation 5 is based on an agitation Reynolds number and its parameters have been estimated using the mean local transfer coefficients. Although the agitation speed obviously remains the same along the height of the basket, the local measurements shown in Figure 9 exhibit a profile in mass transfer; this suggests that a more pertinent characteristic

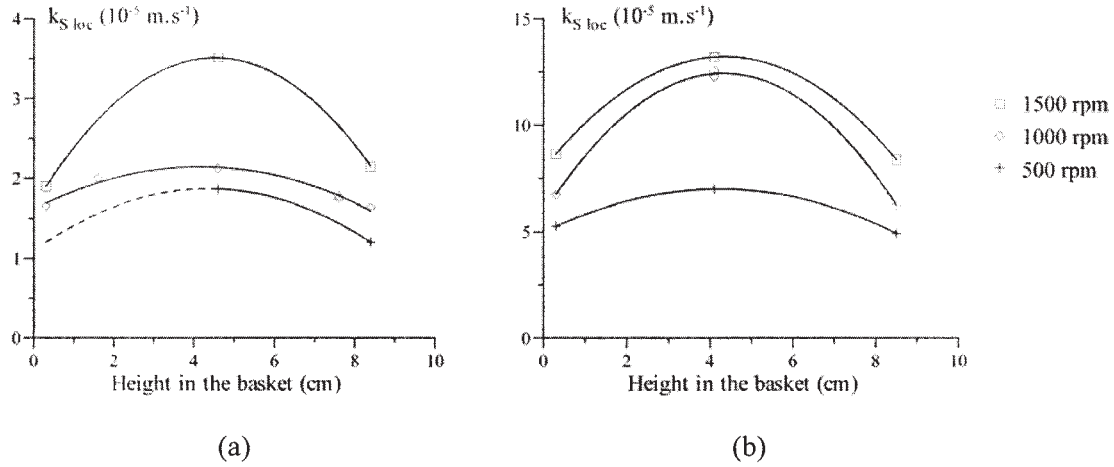

Figure 9. Local mass-transfer coefficients in the catalytic basket.

(a) Water; (b) *n*-heptane.

should be the local velocity of the fluid through the catalytic basket, instead of the agitation speed.

No ideal technique is available to determine local velocities in the catalytic basket because of its small size, on one hand, and the presence of two fluid phases, on the other hand. Two techniques were used in this work: the "catalytic basket simulation device" (CBSD) designed to handle accurately those velocities and to simulate local mass transfer, and the PIV, which allows local measurements, until now in geometrically simple systems.

Solid–liquid transfer in the CBSD

In this experimental device, a 4.5-mm-thick naphtol-packed bed simulated the catalytic basket. A peristaltic pump imposed the fluid velocity. The naphtol mass balance is written as

$$\frac{d(u_o c_L)}{dz} + \frac{A_S}{V\varepsilon} k_S (c_L - c_L^*) = 0 \tag{6}$$

where u_o is the fluid superficial velocity and V and ε are the apparent volume and the external porosity of the packed bed, respectively.

With the boundary condition $c_L = 0$ at $z = 0$ and assuming a constant external area of the particles, Eq. 6 is integrated as

$$\ln\left(1 - \frac{c_L}{c_L^*}\right) = -\frac{k_S A_S}{Q_L} \tag{7}$$

Table 5. Comparison between Mean Local and Global Mass Transfer Coefficients

Rotation Speed (rpm)	Water			Heptane
	$k_{S\,loc}^{mean}$ (10^{-5} m s^{-1})	$k_{S\,glob}$ (10^{-5} m s^{-1})	$\frac{k_{S\,glob} - k_{S\,loc}^{mean}}{k_{S\,loc}^{mean}}$	$k_{S\,loc}^{mean}$ (10^{-5} m s^{-1})
500	1.53	0.99	−35.8%	5.73
1000	1.83	1.35	−26.4%	8.47
1500	2.52	1.69	−32.8%	10.1

where c_L was experimentally very low before c_L^* (from 30 to 100 times lower); therefore Eq. 7 can be simplified as

$$c_L \approx -\frac{c_L^* k_S A_S}{Q_L} \tag{8}$$

A model including axial dispersion was also tested; because the transfer coefficients obtained from the two models differed by only 2%, the axial dispersion could be ignored, according to Wakao and Funazkri (1978).

Figure 12 reports the experimental results obtained in water and *n*-heptane.

Classical correlations in packed beds are of the following forms

$$\begin{cases} \mathrm{Sh} = C\,\mathrm{Re}_p^m \mathrm{Sc}^n \\ \mathrm{Sh} = A + C\,\mathrm{Re}_p^m \mathrm{Sc}^n \end{cases} \tag{9}$$

where $\mathrm{Re}_p = \rho_L u_o d_{pd}/\mu_L$ is the Reynolds number of particle.

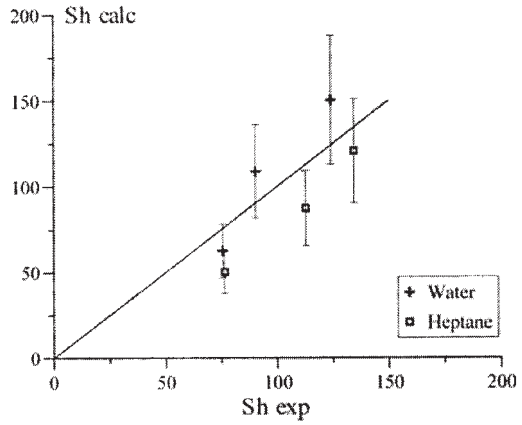

Figure 10. Comparison between experimental and calculated values of Sherwood numbers in catalytic basket.

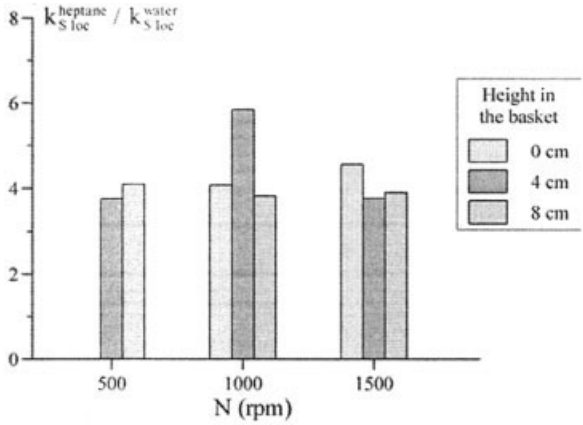

Figure 11. Comparison between local mass-transfer coefficients in *n*-heptane and water at various heights in the basket.

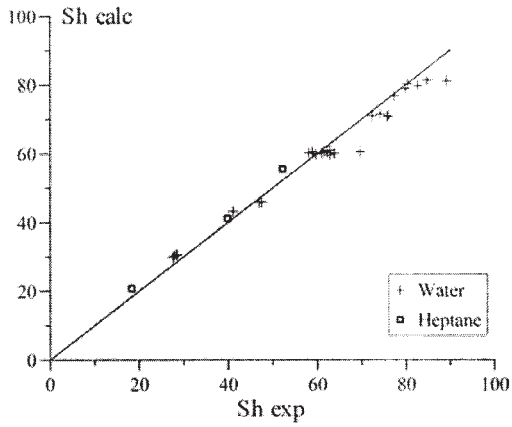

Figure 13. Comparison between experimental and calculated values of Sherwood numbers in CBSD.

Within our experimental range ($2 \leq Re_p \leq 55$; $200 \leq Sc \leq 1200$), the parameter A could be neglected and Eq. 9 becomes

$$Sh = 1.98\, Re_p^{0.37} Sc^{1/3} \tag{10}$$

The parity diagram of this correlation is shown in Figure 13. These results can be compared (cf. Figure 14) with those of Brunjail and Comiti (1990) and Gnielinski (1993), for packed beds of cylinders:

Brunjail and Comiti

$$Sh = 1.24\, Re'^{0.42} Sc^{1/3} \tag{11}$$

where $Re' = (\rho_L u'_1 d_p)/\mu_L$, calculated with the diameter of the sphere whose specific area is identical to that of the naphtol particle (d_p) and the interstitial velocity of the fluid $u'_1 = (u_o\tau)/\varepsilon$; and τ is the tortuosity of the packed bed [1.6 for long cylinders ($L/d = 5.5$)].

Gnielinski

$$Sh = f_a(2 + \sqrt{Sh_{lam}^2 + Sh_{turb}^2}) \tag{12}$$

with

$$Sh_{lam} = 0.0664\, Re_l^{0.5} Sc^{1/3} \tag{13}$$

and

$$Sh_{turb} = \frac{0.037\, Re_l^{0.8} Sc}{1 + 2.443\, Re_l^{-0.1}(Sc^{2/3} - 1)} \tag{14}$$

where $Re_l = (\rho_L u_i d_{pa})/\mu_L$ is the Reynolds number and f_a is a form factor (1.6 for cylinders with $0.24 < L/d < 1.2$).

Our correlation is consistent with published results, especially with Brunjail, although the latter (Gnielinski) deals with cylinders shorter ($L/d = 1.2$) and the former (Brunjail) with cylinders longer ($L/d = 5.5$) than those we used ($L/d = 3$).

Should our correlation (Eq. 10) be applicable in the Robinson–Mahoney reactor, we could use it to deduce the interstitial velocity u_i of the liquid through the catalytic basket from the measured $k_{S\,loc}$ values (cf. Figure 9). These velocities are shown in Figure 15.

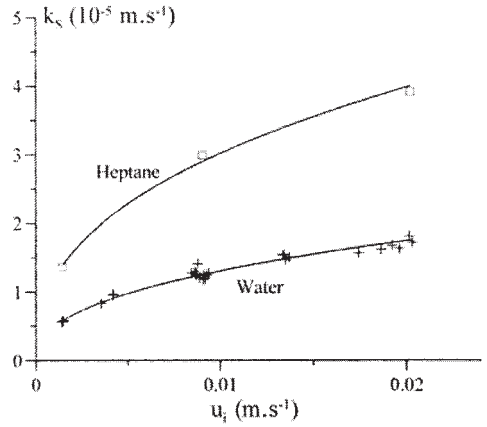

Figure 12. Mass-transfer coefficients in CBSD vs. interstitial velocity.

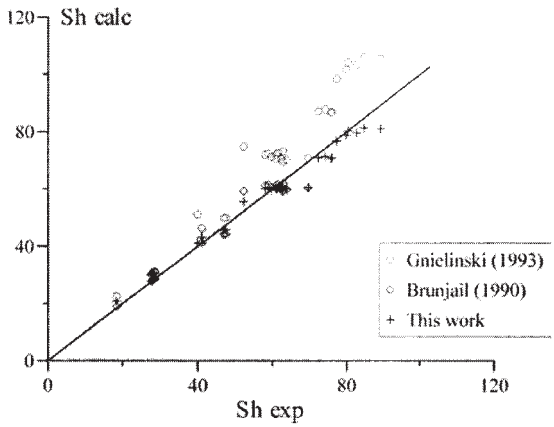

Figure 14. Comparison between experimental and published values of Sherwood numbers.

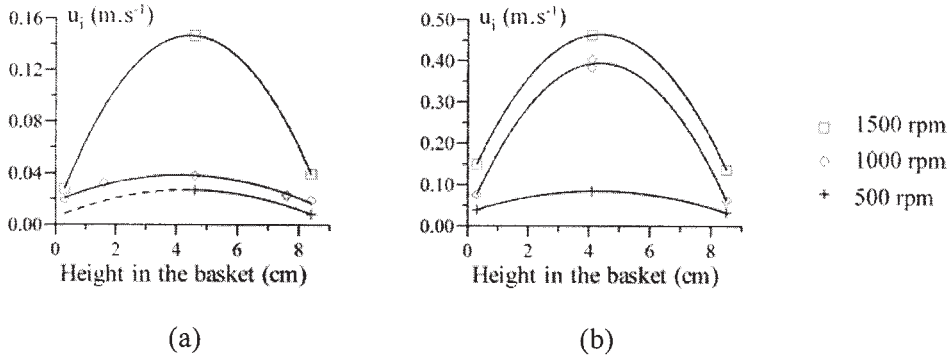

Figure 15. Interstitial velocities in the catalytic basket, deduced from CBSD measurements.

(a) Water; (b) *n*-heptane.

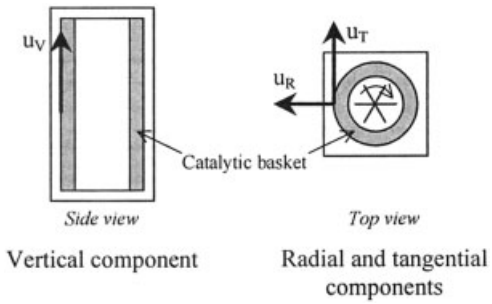

Figure 16. PIV velocities measurements.

To validate the mass-transfer measurements, it was necessary to confirm these velocities independently, and thus we used the particle image velocimetry technique.

Velocimetry measurements in the RM reactor

As described above, implementation of PIV measurements allowed the determination of velocities at a distance of 2 mm outside the basket wall, along three directions (Figure 16).

The three velocity components (u_R, u_T, u_V) were obtained along vertical profiles at midangular distance between baffles. Mean velocity profiles for three rotation speeds are presented in Figure 17. Even with 200 samples the mean average velocity profiles are not smooth. PIV analysis succeeds about 90% of the time, and thus this is not a predominant factor that contributes to fluctuations in the velocity profile. The catalytic basket contains some rows of cylinders disposed randomly, which might contribute substantially to these fluctuations.

The vertical component of velocity exhibits positive values (upward velocities) in the upper half of the basket and negative values (downward velocities) in the lower one. The tangential component fluctuates, but always with positive values, indicating the pseudo-circular flow around the basket. The radial component has a maximal zone toward center of the basket, with positive values (flow exiting the basket), and some negative values at extremities (flow reentering the basket). Moreover, the shapes of these profiles are similar, irrespective of the rotation speed; amplitude alone is modified. These data generate the flow pattern shown in Figure 18.

As stated earlier, velocity is a key parameter concerning mass transfer. An important point to emphasize is that the normal and tangential components are the main components of the velocity inside the basket. The vertical component assumes some importance between the external side of the basket and the reactor wall. Actually, all the streams exiting the basket flow together in the annular space between the basket and the reactor wall, and contribute to the vertical velocity component; this component is therefore not representative for the fluid behavior within the basket.

Consequently, the pertinent comparison is to be done between interstitial velocity u_i, deduced from CBSD experiments, and the velocity projection on the horizontal plane ($u_{RT} = \sqrt{u_R^2+u_T^2}$), measured by PIV; this comparison is shown in Figure 19.

The good agreement between these two independent sets of

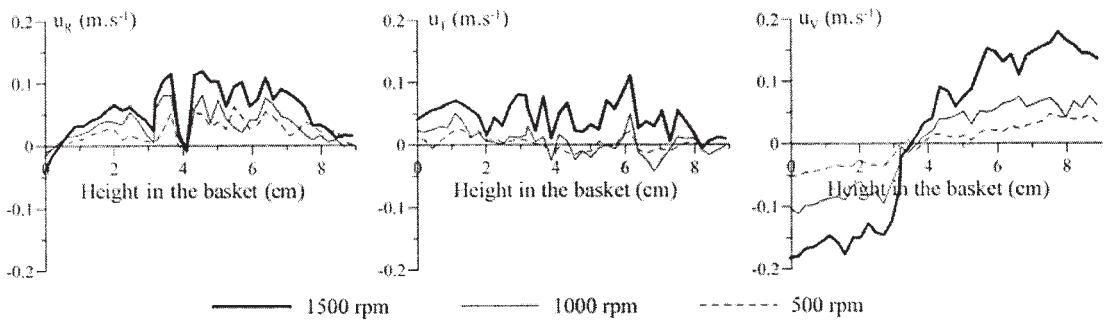

Figure 17. Velocities profiles for three rotation speeds (500, 1000, and 1500 rpm).

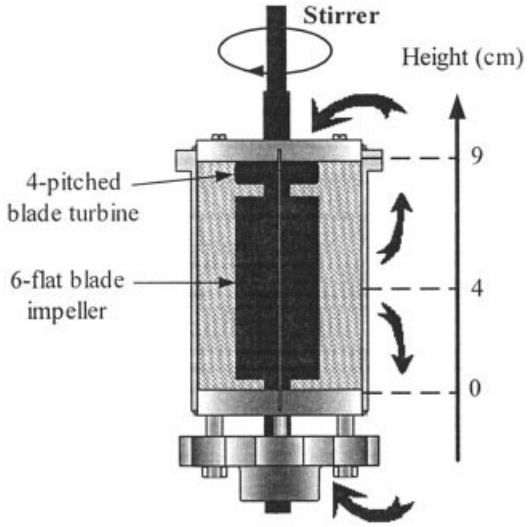

Figure 18. Flow pattern in the Robinson–Mahoney reactor.

experiments validates the mass-transfer measurements in the Robinson–Mahoney reactor (Eq. 5). That validation is confirmed in water; however, the corresponding experiments in heptane should be carried out in further development of this work.

Conclusion

A first correlation for global mass transfer as a function of agitation speed was developed for the Robinson–Mahoney catalytic reactor. It will be a useful tool for predicting the behavior of this particular kinetic investigation reactor. Then, a second correlation established in a specific device (CBSD) correlated measured local solid–liquid mass transfer with liquid velocities for two different liquids. Velocity values have been confirmed by PIV measurements (only in water); further experiments using *n*-heptane would extend the applicability of the correlation. Our results highlight a mass-transfer coefficient profile along the height of the catalytic basket, allowing a pertinent choice of catalyst location within the basket and/or suggesting changes of structured basket to avoid top and bottom effects (such as filling basket top and bottom with inert particles). That second correlation—linking mass-transfer coefficient to interstitial velocity inside the basket—would allow, for instance, determination of velocities calculated with computational fluid dynamics, to predict the liquid/solid mass-transfer limitations without any experiment. Finally, the comparison between mass-transfer coefficients found in *n*-heptane (that is, simulating gas oil under hydrocracking conditions) and mean kinetics parameters published by Schweitzer (1998) shows that mass-transfer coefficients are hundred of times higher, which implies that the hydrocracking apparent reaction rate is not controlled by solid–liquid mass transfer in this reactor and that error with respect to intrinsic kinetics was about 1%.

Acknowledgments

The authors thank Institut Français du Pétrole for financial support. In particular we thank P. Galtier and J. M. Schweitzer for fruitful discussions. E. Bourgeat-Lami, Laboratoire de Chimie des Procédés de Polymérisation, CPE-Lyon, Villeurbanne (France) was helpful in the PMMA particle synthesis.

Notation

A_S = total external area of particles, m^2
A_R, A_T, A_V = radial, tangential, vertical axes
c_L = concentration of naphtol in the bulk liquid, mol m^{-3}
c_L^* = equilibrium concentration of naphtol in the bulk liquid, mol m^{-3}
c_{Lo} = concentration of naphtol in the bulk liquid at time t_o, mol m^{-3}
d_t = impeller diameter, m
d_p = diameter of the sphere of same specific area as that of the particle, m
d_{pa} = diameter of the sphere of same area as that of the particle, m
D_L = diffusivity of naphtol in liquid, $m^2\ s^{-1}$
f_a = form factor
k_S = solid–liquid mass-transfer coefficient, m s^{-1}
$k_{S\,glob}$ = global value of solid–liquid mass-transfer coefficient, m s^{-1}
$k_{S\,loc}$ = local value of solid–liquid mass-transfer coefficient, m s^{-1}
$k_{S\,loc}^{mean}$ = mean value of local solid–liquid mass-transfer coefficients, m s^{-1}
N = agitation speed, tr s^{-1}
Q_G = gas volumic flow, $m^3\ s^{-1}$
Q_L = liquid volumic flow, $m^3\ s^{-1}$

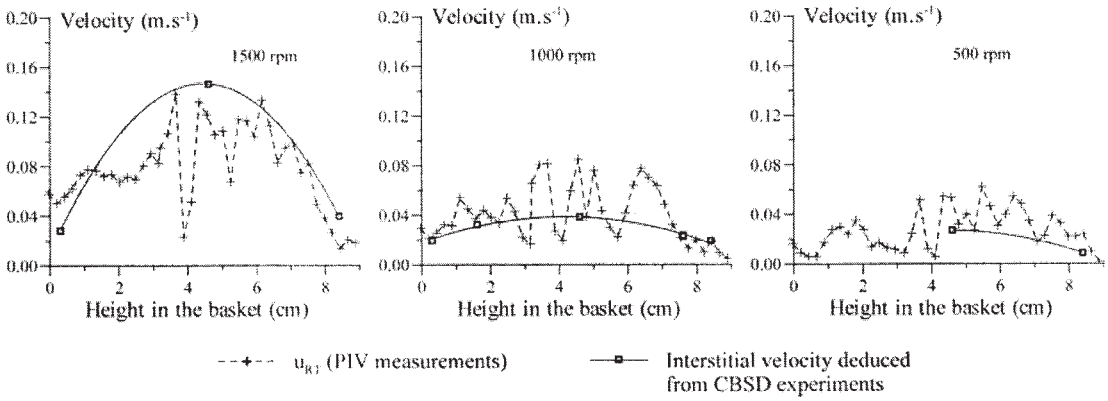

Figure 19. Horizontal velocity (u_{RT}) profiles (in water) obtained by PIV measurements and deduced from CBSD experiments.

Re_t = Reynolds number of the turbine, $\mathrm{Re}_t = N\rho_L d^2/\mu_L$
Re_p = Reynolds number of the particle, $\mathrm{Re}_p = \rho_L u_o d_{pa}/\mu_L$
Re' = Reynolds number, $\mathrm{Re}' = \rho_L u'_1 d_p/\mu_L$ (Eq. 11)
Re_l = Reynolds number, $\mathrm{Re}_l = \rho_L u_i d_{pa}/\mu_L$ (Eq. 12)
Sc = Schmidt number, $\mathrm{Sc} = \mu_L/\rho_L D_L$
Sh = Sherwood number, $\mathrm{Sh} = k_S d_{pa}/D_L$
Sh_{lam} = Sherwood number in laminar regime
Sh_{turb} = Sherwood number in turbulent regime
t = time, s
u_i = interstitial velocity of the fluid, m s^{-1}
u_o = superficial velocity of the fluid, $u_o = u_i\varepsilon = (Q_L/\Omega)$, m s^{-1}
u'_1 = interstitial velocity of the fluid $u'_1 = u_o\tau/\varepsilon$, m s^{-1}
u_R = radial component of the velocity, m s^{-1}
u_T = tangential component of the velocity, m s^{-1}
u_V = vertical component of the velocity, m s^{-1}
V_L = volume of the liquid phase, m^3
V = apparent volume of the packed bed, m^3

Greek letters

ε = void fraction in the packed bed
μ_L = viscosity of liquid phase, Pa·s
ρ_L = specific gravity of liquid phase, kg m^{-3}
τ = tortuosity of the packed bed
Ω = inlet area in the CBSD, m^2

Literature Cited

Brunjail, D., and J. Comiti, "Mass Transfer and Energy Aspects for Forced Flow through Packed Beds of Long Cylindrical Particles," *Chem. Eng. J.*, **45**(2), 123 (1990).

Carberry, J. J., "Designing Laboratory Catalytic Reactors," *J. Ind. Eng. Chem.*, **56**(11), 39 (1964).

Dudukovic, M. P., F. Larachi, and P. L. Mills, "Multiphase Catalytic Reactors: A Perspective on Current Knowledge and Future Trends," *Catal. Rev. Sci. Eng.*, **44**(1), 123 (2002).

Dutta, N. N., and V. G. Pangarkar, "Solid–Liquid Mass Transfer in Three Phase Fluidized Beds: Some Scale-Up Effects," *Chem. Eng. Commun.*, **119**, 55 (1993).

Evans, G. C., and C. F. Gerald, "Mass Transfer from Benzoic Acid Granules to Water in Fixed and Fluidized Beds at Low Reynolds Numbers," *Chem. Eng. Prog.*, **49**, 135 (1953).

Forissier, M., M. Mitrovic, I. Pitault, and D. Ronze, "Influence of the Residence Time Distribution Knowledge on Gas–Liquid Mass Transfer Coefficient Estimation," *Réc. Prog. Génie Proc.*, **15**(79), 363 (2001).

Gnielinski, V., "Fluid–Particle Heat Transfer in Flow through Beds of Solids," *VDI Heat Atlas*, VDI-Verlag GmbH, Düsseldorf, Germany, pp. Gh1–Gh2 (1993).

Grisafi, F., A. Brucato, and L. Rizzuti, "Solid–Liquid Mass Transfer Coefficients in Gas–Solid–Liquid Agitated Vessels," *Can. J. Chem. Eng.*, **76**(3), 446 (1998).

Hayduk, W., and H. Laudie, "Prediction of Diffusion Coefficients for Nonelectrolytes in Dilute Aqueous Solutions," *AIChE J.*, **20**(3), 611 (1974).

Kawakami, K., S. Ura, and K. Kusunoki, "The Effectiveness Factor of a Catalyst Pellet in the Liquid-Phase Hydrogenation of Styrene," *J. Chem. Eng. Jpn.*, **9**(5), 392 (1976).

Kenney, C. N., and W. Sedriks, "Effectiveness Factors in a Three-Phase Slurry Reactor. Reduction of Crotonaldehyde over a Palladium Catalyst," *Chem. Eng. Sci.*, **27**(11), 2029 (1972).

Lafontaine, R. F., and I. C. Shepherd, "Particle Image Velocimetry Applied to a Stirred Vessel," *Exp. Therm. Fluid Sci.*, **12**, 256 (1996).

Lamberto, D. J., M. M. Alvarez, and F. Z. Muzzio, "Experimental and Computational Investigation of the Laminar Flow Structure in a Stirred Tank," *Chem. Eng. Sci.*, **54**(7), 919 (1999).

Levins, D. M., and J. R. Glastonbury, "Particle–Liquid Hydrodynamics and Mass Transfer in a Stirred Vessel. 2. Mass Transfer," *Trans. IChemE.*, **50**(2), 132 (1972).

Lourenco, L. M., and A. Krothapalli, "On the Accuracy of Velocity and Vorticity Measurements with PIV," *Exp. Fluids*, **18**, 421 (1995).

Mahoney, J. A., "Laboratory Reactors for Mixed Phase Catalytic Studies," *NATO Adv. Study Inst. Ser. E*, **52**, 487 (1981).

Mahoney, J. A., K. K. Robinson, and E. C. Myers, "Catalyst Evaluation with the Gradientless Reactor," *Chemtech*, **8**(12), 758 (1978).

Nosier, S. A., A. El-Kayar, H. A. Farag, and G. H. Sedahmed, "Solid–Liquid Mass Transfer at Gas Sparged Fixed Bed of Raschig Rings," *Int. Commun. Heat Mass Transfer*, **24**(5), 733 (1997).

Ohta, H., S. Goto, and H. Teshima, "Liquid-Phase Oxidation of Phenol in a Rotating Catalytic Basket Reactor," *Ind. Eng. Chem. Fundam.*, **19**(2), 180 (1980).

Pangarkar, V. G., A. A. Yawalkar, M. M. Sharma, and A. A. C. M. Beenackers, "Particle–Liquid Mass Transfer Coefficient in Two-/Three-Phase Stirred Tank Reactors," *Ind. Eng. Chem. Res.*, **41**, 4141 (2002).

Patil, V. K., J. B. Joshi, and M. M. Sharma, "Solid–Liquid Mass-Transfer Coefficient in Mechanically Agitated Contactors," *Chem. Eng. Res. Des.*, **62**(4), 247 (1984).

Sano, Y., N. Yamaguchi, and T. Adachi, "Mass Transfer Coefficients for Suspended Particles in Agitated Vessels and Bubble Columns," *J. Chem. Eng. Jpn.*, **7**(4), 255 (1974).

Schweitzer, J. M., "*Modélisation cinétique des réactions catalytiques d'hydrocraquage par la théorie des évènements constitutifs*," PhD Thesis, University of Lyon, France (1998).

Schweitzer, J. M., P. Galtier, and D. Schweich, "A Single Events Kinetic Model for the Hydrocracking of Paraffins in a Three Phase Reactor," *Chem. Eng. Sci.*, **54**(13–14), 2441 (1999).

Sedahmed, G. H., A. M. El-Kayar, H. A. Farag, and S. A. Nosier, "Liquid–Solid Mass Transfer in Packed Beds of Raschig Rings with Upward Two-Phase (Gas–Liquid) Flow," *Chem. Eng. J.*, **62**(1), 61 (1996).

Simoens, S., and M. Ayrault, "Concentration Flux Measurements of a Scalar Quantity in Turbulent Flow," *Exp. Fluids*, **16**(3–4), 273 (1994).

Trasobares, S., M. A. Callejas, A. M. Benito, M. T. Martinez, D. Severin, and L. Brouwer, "Kinetics of Conradson Carbon Residue Conversion in the Catalytic Hydroprocessing of a Maya Residue," *Ind. Eng. Chem. Res.*, **37**(1), 11 (1998).

Turek, F., R. K. Chakrabarti, R. Lange, R. Geike, and W. Flock, "On the Experimental Study and Scale-Up of Three-Phase Catalytic Reactors," *Chem. Eng. Sci.*, **38**(2), 275 (1983).

Vanrysselberghe, V., and G. F. Froment, "Hydrodesulfurization of Dibenzothiophene on a $CoMo/Al_2O_3$ Catalyst: Reaction Network and Kinetics," *Ind. Eng. Chem. Res.*, **35**(10), 3311 (1996).

Vincont, J. Y., S. Simoens, M. Ayrault, and J. Wallace, "Passive Scalar Dispersion in a Turbulent Boundary Layer from a Line Source at the Wall and Downstream of an Obstacle," *J. Fluid Mech.*, **424**, 127 (2000).

Wakao, N., and T. Funazkri, "Effect of Fluid Dispersion Coefficients on Particle-to-Fluid Mass Transfer Coefficients in Packed Beds," *Chem. Eng. Sci.*, **33**(10), 1375 (1978).

Weekman, V. W., "Laboratory Reactors and Their Limitations," *AIChE J.*, **20**(5), 833 (1974).

Wilke, C. R., and P. Chang, "Correlation of Diffusion Coefficients in Dilute Solutions," *AIChE J.*, **1**(2), 264 (1955).

Willert, C. E., and M. Gharib, "Digital Particle Image Velocimetry," *Exp. Fluids*, **10**(3), 181 (1991).

Zarraa, M. A., M. Z. El-Abd, Y. A. El-Tawil, H. A. Farag, and G. H. Sedahmed, "Liquid–Solid Mass Transfer in a Batch-Packed Bubble Column," *Chem. Eng. J.*, **54**(1), 51 (1994).

Manuscript received Feb. 5, 2004, and revision received Oct. 21, 2004.